Comparison of Dynamic Differential Evolution and Genetic Algorithm for MIMO-WLAN Transmitter Antenna Location in Indoor Environment

Shu-Han Liao · Chien-Ching Chiu · Min-Hui Ho

Abstract A novel optimization procedure for the location of the transmitter in 3×3 multiple input multiple output (MIMO) wireless local area network (WLAN) wireless communication systems is presented. The optimal antenna location for maximizing the channel capacity is searched by dynamic differential evolution (DDE) and genetic algorithm (GA). There are two different receiver locations considered in the simulation. The receivers are located with uniform intervals distribution either on the tables or in the whole indoor environment. Numerical results show that the performance for increasing channel capacity by DDE algorithm is better than that by GA.

Keywords MIMO-WLAN · DDE · GA · Channel capacity

1 Introduction

In recent years there has been a growing interest in the development of potentially mass-producible application systems using millimeter waves, such as wireless LAN (local area networks) systems [1]. To develop millimeter-wave wireless LAN systems, however, we need to know the reflection and transmission characteristics in millimeter-wave bands so that we can evaluate indoor multipath propagation characteristics and the interactions of millimeter waves with various objects.

This paper addresses basic issues regarding the wireless LAN systems that operate in the 60 GHz band as part of the fourth-generation (4G) system [2]. The 60 GHz band provides 7 GHz of unlicensed spectrum with a potential to develop wireless communication systems with multi Gbps throughput. The IEEE 802.11 standard committee [3], one of the major organizations in WLAN specifications development, established the IEEE 802.11ad task group to develop an amendment for the 60 GHz WLAN systems.

S.-H. Liao · C.-C. Chiu (✉)· M.-H. Ho
Department of Electrical Engineering, Tamkang University, Tamsui Dist., Taiwan, ROC
e-mail: chiu@ee.tku.edu.tw

All wireless systems must be able to deal with the challenges of operating over a multipath propagation channel, where object in the environment can cause multiple reflections to arrive at the receiver. In general, effective antenna selection and deployment strategies are important for reducing BER in indoor wireless systems [4,5]. GA shows a good performance for indoor network planning, and this is also presented in [6]. In [7] the model proposes a 2-D ray tracing prediction technique associated with a real-coded mono-objective genetic algorithm (GA). The GA provides results for antenna position optimization that maximizes the lower field values. In this paper, the best transceiver locations on the WLAN communication systems are presented. Based on the channel capacity formula, the channel capacity instead of signal power is chosen as the cost function. Then this location problem is transformed into the optimization problem. Since this optimization problem is often highly nonlinear and non-differentiable, dynamic differential evolution (DDE) and GA is use to search the transmitter location to maximizing the channel capacity of the communication system. Moreover, different values of dielectric constant and conductivity of materials for different frequency is carefully considered in channel calculation.

The remainder of this paper is organized as follows. In Sect. 2, channel modeling and system description are presented. Several numerical results are included in Sect. 3, while Sect. 4 concludes the paper.

2 Channel Modeling and System Description

2.1 Channel Modeling

The following two steps are used to calculate the multi-path radio channel.

2.1.1 Frequency Responses for Sinusoidal Waves by SBR/Image Techniques

The SBR/Image method can deal with high frequency radio wave propagation in the complex indoor environment [8,9]. It conceptually assumes that many triangular ray tubes are shot from the transmitting antenna (TX), and each ray tube, bouncing and penetrating in the environment is traced in the indoor multi-path channel. If the receiving antenna (RX) is within a ray tube, the ray tube will have contributions to the received field at the RX, and the corresponding equivalent source (image) can be determined. By summing all contributions of these images, we can obtain the total received field at the RX. In real environment, external noise in the channel propagation has been considered. The depolarization yielded by multiple reflections, refraction and first order diffraction are also taken into account in our simulations. Note that the different values of dielectric constant and conductivity of materials for different frequencies are carefully considered in channel modeling.

A ray-tracing technique is a good technique to calculate channel frequency response for wireless communication [10–15]. As a result, we develop a ray-tracing technique to model channel for our simulations. Using ray-tracing techniques to predict channel characteristic is effective and fast [8,9,16]. Thus, a ray-tracing channel model is developed to calculate the channel matrix of UWB system. Flow chart of the ray-tracing process is shown in Fig. 1. It conceptually assumes that many triangular ray tubes (not rays) are shot from a transmitter. Here the triangular ray tubes whose vertexes are on a sphere are determined by the following method. First, we construct an icosahedron which is made of 20 identical equilateral triangles. Then, each triangle of the icosahedron is tessellated into a lot of smaller equilateral triangles.
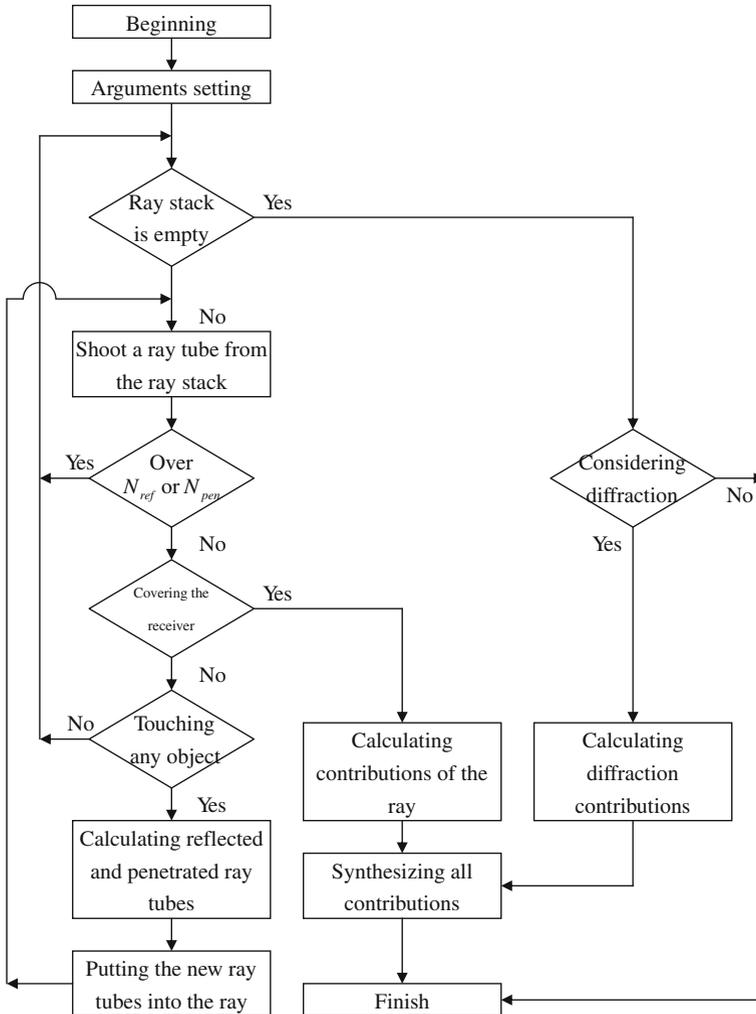
Fig. 1 The flow chart of the ray-tracing process

Finally, these small triangles are projected on to the sphere and each ray tube whose vertexes are determined by the small equilateral triangle is constructed [17].

For each ray tube bouncing and penetrating in the environments, we check whether reflection times and penetration times of the ray tube are larger than the numbers of maximum reflection N_{ref} and maximum penetration N_{pen}, respectively. If it no, we check whether the receiver falls within the reflected ray tube. If it yes, the contribution of the ray tube to the receiver can be attributed to an equivalent source (i.e. image source). In other words, a specular ray going to receiver exists in this tube and this ray can be thought as launched from an image source. Moreover, the field diffracted from illuminated wedges of the objects in the environment is calculated by uniform theory of diffraction (UTD) [18]. Note that only first diffraction is considered in this paper, because the contribution of second diffraction is very small in the analysis. As a result, the corresponding equivalent source (image) can be

determined. Some details can refer to literature [19]. By using these images and received fields, the channel frequency response can be obtained as following

$$H(f) = \sum_{p=1}^{N_p} a_p(f)e^{j\theta_p(f)} \tag{1}$$

where p is the path index, N_p is the total number of paths, f is the frequency of sinusoidal wave, $\theta_p(f)$ is the pth phase shift and $a_p(f)$ is the pth receiving magnitude. Note that the transmitting and receiving antenna are modeled as a UWB antenna with simple omni-directional radiation pattern and vertically polarized. The channel frequency response of UWB can be calculated from Eq. (1) in the frequency range of UWB.

2.1.2 Inverse Fast Fourier Transform (IFFT) and Hermitian Processing

The frequency response is transformed to the time domain by using the inverse fast Fourier transform with the Hermitian signal processing [20]. By using the Hermitian processing, the pass-band signal is obtained with zero padding from the lowest frequency down to direct current (DC), taking the conjugate of the signal, and reflecting it to the negative frequencies. The result is then transformed to the time domain using IFFT [21]. Since the signal spectrum is symmetric around DC. The resulting doubled-side spectrum corresponds to a real signal in the time domain. Therefore, the time domain impulse response of the equivalent baseband can be written as follows [22]:

$$h_b(t) = \sum_{m=1}^{M_T} \alpha_m \delta(t - \tau_m) \tag{2}$$

where m is the path index and M_T is the total number of paths. δ () is the Dirac delta function. α_m and τ_m are the channel gain and time delay for the mth path, respectively.

Using ray-tracing approaches to predict channel characteristic is effective and fast, and the approaches are also usually applied to MIMO channel modeling in recent years [23,24]. Thus, a ray-tracing technique is developed to calculate the channel matrix of MIMO system is the paper.

2.2 System Description

The received signal for a time-invariant narrowband system combining with MIMO (MIMO-NB system) is described as follows [25]:

$$\mathbf{Y} = \mathbf{HX} + \mathbf{W} \tag{3}$$

$$\mathbf{H} = \begin{bmatrix} h_{11} & h_{12} & h_{13} & \dots h_{1N_t} \\ h_{21} & h_{22} & h_{33} & \dots h_{2N_t} \\ h_{21} & h_{22} & h_{33} & \dots h_{3N_t} \\ \vdots & \vdots & \vdots & \ddots \vdots \\ h_{N_r 1} & h_{N_r 2} & h_{N_r 3} & \cdots h_{N_r N_t} \end{bmatrix} \tag{4}$$

where $\mathbf{X}$, $\mathbf{Y}$ and $\mathbf{W}$ denote the $N_t \times 1$ transmitted signal vector, the $N_r \times 1$ received signal vector and the $N_r \times 1$ zero mean additive white Gaussian noise vector at a symbol time, respectively, $\mathbf{H}$ is the $N_r \times N_t$ channel matrix and h_{ij} is the complex channel gain from the jth transmitting antenna to the ith receiving antenna.
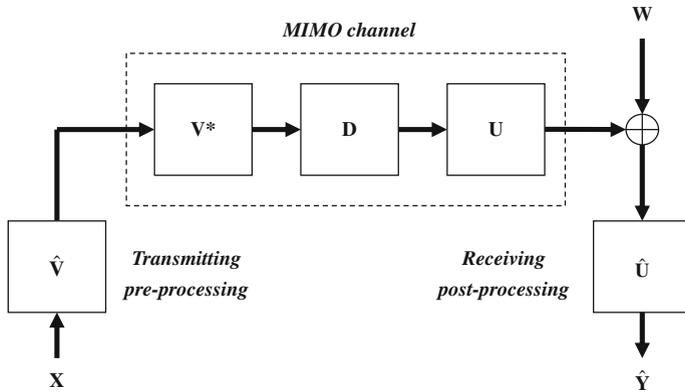
Fig. 2 A matrix representation of MIMO-NB system

From linear algebra theory, every linear transformation can be represented as a composition of three operations: a rotation operation, a scaling operation, and another rotation operation [26]. As a result, the channel matrix H can be expressed by singular value decomposition (SVD) as follows:

$$\mathbf{H} = \mathbf{UDV}^* \tag{5}$$

where $\mathbf{U}$ and $\mathbf{V}^*$ are the $N_r \times N_r$ and $N_t \times N_t$ unitary matrices, $\mathbf{D}$ is a $N_r \times N_t$ rectangular matrix whose diagonal elements are non-negative real values and other elements are zero and the symbol $*$ in Eq. (5) stands for the conjugate transpose or Hermitian operation.

MIMO is capable of signal processing at the transmitter and receiver to produce the set of received signals with highest overall capacity. A matrix representation of MIMO-NB system is shown in Fig. 2. In this figure, a linear signal processing operation $\hat{\mathbf{V}}$ is multiplied by the transmitted signal vector $\mathbf{X}$ to produce a new set of signals. The new set of signals is fed further into the MIMO channel. Finally, another linear signal processing operation $\hat{\mathbf{U}}$ is multiplied by the incoming signal propagating through the channel. The final output signal vector $\hat{\mathbf{Y}}$ is expressed as follow:

$$\hat{\mathbf{Y}} = \hat{\mathbf{U}}(\mathbf{UDV}^*)\hat{\mathbf{V}}\mathbf{X} + \hat{\mathbf{U}}\mathbf{W} \tag{6}$$

Note that there is no adding or subtracting of any signal power in the system, because $\hat{\mathbf{V}}$ and $\hat{\mathbf{U}}$ are both unitary matrix.

If channel state information (CSI) is known for receiver, the channel capacity of the MIMO-NB system can be written in an equivalent matrix notation for $N_t \geq N_r$ as follows:

$$C^{NB} = B \log_2 \left(\det \left(I + \frac{SNR_t}{N_t} DD^* \right) \right) \tag{7}$$

where $\mathbf{I}$ is an appropriately sized identity matrix. Using the relationship of $\mathbf{D} = \mathbf{U}^*\mathbf{HV}$, Eq. (7) can be rewritten as follows:

$$C^{NB} = B \log_2 \left(\det \left(I + \frac{SNR_t}{N_t} U^* H H^* U \right) \right) \tag{8}$$

Since $\mathbf{U}$ is an unitary matrix, and it does not change the value of the determinant of the matrix that they multiply. Thus, Eq. (8) can be rewritten as follows [27–29]:

$$C^{NB} = B \log_2 \left(\det \left(I + \frac{SNR_t}{N_t} HH^* \right) \right) \quad (9)$$

The equation is especially effective to calculate MIMO capacity in a mathematical software package, since the channel capacity needs channel state information (CSI) for the receiver only.

By the ray-tracing technique, all the frequency responses inside the bandwidth of WLAN between any transmitter and receiver antennas are calculated. Then, MIMO channel capacity of WLAN transmission can be calculated as summation of the channel capacity of the narrowband at each discrete frequency point. Thus, the channel capacity (bandwidth efficiency) can be written as

$$C^{WLAN} = \frac{1}{BW} \sum_{k=1}^{N_f} C_k^{narrowband} \text{ (bits/sec/Hz)} \quad (10)$$

where BW is the total bandwidth of WLAN and N_f are the numbers of frequency components.

2.3 Dynamic Differential Evolution (DDE)

DDE algorithm starts with an initial population of potential solutions that is composed by a group of randomly generated individuals which represents antenna location of the transmitters. Each individual in DDE algorithm is a D-dimensional vector consisting of D optimization parameters. The initial population may be expressed by $\{x_i : i = 1, 2, \ldots, Np\}$, where Np is the population size. After initialization, DDE algorithm performs the genetic evolution until the termination criterion is met. DDE algorithm, like other EAs, also relies on the genetic operations (mutation, crossover and selection) to evolve generation by generation. The flowchart of the DDE algorithm is shown in Fig. 3. DDE algorithm goes through six procedures as follows:

I. Initialize a starting population: DDE algorithm is initialized with a population that is composed by a group of randomly generated candidate individuals. Individuals in DDE algorithm represent a set of D-dimensional vectors in the parameter space for the problem, $\{x_i : i = 1, 2, \ldots, Np\}$, where D is the number of parameters to be optimized and Np is the population size.

II. Evaluate the population using cost function: After initialization, DDE algorithm evaluates the cost function for each individual in the population.

III. Perform mutation operation to generate trial vectors: The mutation operation of DDE algorithm is performed by arithmetical combination of individual. For each parameter vector x_i^g of the parent generation, a trial vector v_i^{g+1} is generated according to following equation:

$$\begin{aligned} &(V_j^{g+1})i = (X_j^g)i + F \cdot [(X_{best}^g)i - (X_j^g)i] + \lambda \cdot [(X_{r1}^g)i - (X_{r2}^g)i], \\ &r1, r2 \in [0, N_p - 1], \quad r1 \neq r2 \end{aligned} \quad (11)$$

where F and λ are the scaling factors associated with the vector differences $(X_{best}^g - X_j^g)$ and $(X_{r1}^g - X_{r2}^g)$, respectively. The disturbance vector V due to the mutation mechanism consists of parameter vector X_j^g, the best particle X_{best}^g and two randomly selected vectors. As compared to typical DE [30], the convergence can be accelerated by (11).

IV. Perform crossover operation with probability of crossover Cr to deliver crossover vectors: The crossover operation in DDE algorithm is performed to increase the diversity
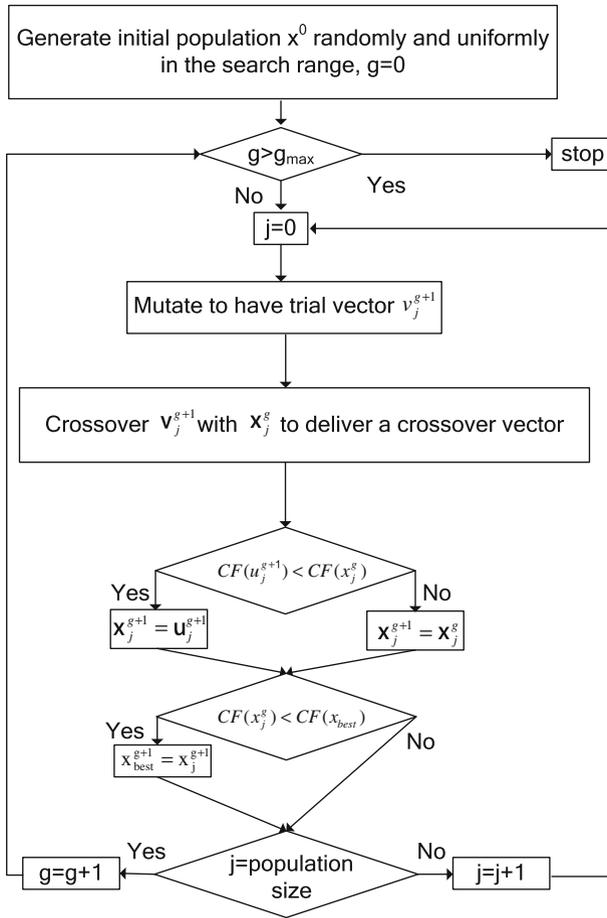
Fig. 3 The flow chart of the dynamic differential evolution (DDE)

of the parameter vectors. This operation is similar to the crossover process in GAs. However, the crossover operation in DDE algorithm just allows to deliver the crossover vector u_i by mixing component of the current vector x_i^g and the trial vector v_i^{g+1}. It can be expressed as:

$$u_i^{g+1}(j) = \begin{cases} v_i^{g+1}(j), & if \ Rand(j) < Cr \\ x_i^g(j), & otherwise \end{cases} \tag{12}$$

where Cr is the probability of crossover, $Cr \in (0, 1)$. $Rand(j)$ is the random number generated uniformly between 0 and 1.

V. Perform selection operation to produce offspring: Selection operation is conducted by comparing the parent vector x_i^g with the crossover vectors u_i^{g+1}. The vector with smaller cost function value is selected as a member of the next generation. Explicitly, the selection operation for the minimization problem is given by:

$$x_i^{g+1} = \begin{cases} x_i^{g+1} & if \ OF\left(u_i^g\right) < OF\left(x_i^g\right) \\ x_i^g & otherwise \end{cases} \tag{13}$$

The DDE algorithm is carried out in a dynamic way: each parent individual would be replaced by its offspring if the offspring has obtained a better cost function value than its parent. Thus, DDE algorithm can respond the progress of population status immediately and yield faster convergence speed than the typical DE algorithm [30]. Based on the convergent characteristic of DDE algorithm, we are able to reduce the numbers of cost function evaluation and find the solution efficiently.

VI. Stop the process and obtain the best individual if the termination criterion is satisfied, else go to step II.

The key distinction between a DDE algorithm and a typical DE is on the population updating mechanism. In a typical DE, all the update actions of the population are performed at the end of the generation, of which the implementation is referred to as static updating mechanism. Alternatively, the updating mechanism of DDE algorithm is carried out in a dynamic way: each parent individual would be replaced by her offspring if the offspring has obtained a better cost function value than its parent. Thus, DDE algorithm can respond the progress of population status immediately and to yield faster convergence speed than the typical DE. Based on the convergent characteristic of DDE algorithm, we are able to reduce the numbers of cost function evaluation.

In the synthesis procedure, the DDE is used to minimize the following cost function (CF):

$$CF = \frac{1}{\frac{1}{BW} \sum_{k=1}^{N_f} C_k^{narrowband}} \tag{14}$$

where cost function is the inverse of channel capacity for WLAN system. DDE is used to search the transmitter antenna position to maximize the channel capacity of the communication system. This SBR/Image method technique is used to calculate the WLAN channel impulse response for each location of the receiver. Based on the channel impulse response, the number of multipath components, the root mean square (RMS) delay spread τ_{RMS} and the mean excess delay τ_{MED} are computed. The DDE algorithm iteratively generates a new population that offspring from the previous population through the application of the reproduction by mutation and replacement operators. In our simulation, when the cost function is bigger than the threshold value or DDE do not find a better individual within 300 successive generations. The DDE will be terminated and a solution is then obtained.

2.4 Genetic Algorithm (GA)

Genetic algorithm is the global numerical optimization methods based on genetic recombination and evaluation in nature [31,32]. They use the iterative optimization procedures, which start with a randomly selected population of potential solutions. Then gradually evolve toward a better solution through the application of the genetic operators. GA typically operates on a discretized and coded representation of the parameters rather than on the parameters themselves. These representations are often considered to be "chromosomes", while the individual element, which constitutes chromosomes, is the "gene". Simple but often very effective chromosome representations for optimization problem involving several continuous parameters can be obtained through the juxtaposition of discretized binary representations of the individual parameter.

We regulate the transmitter antenna location of the indoor environment to maximize the channel capacity. The GA starts with a population containing a total of G_P candidates (i.e., G_P is the population size). Each candidate is described by a chromosome. Then the initial population can simply be created by taking G_P random chromosomes. GA iteratively gener-

ates a new population, which is derived from the previous population through the application of the reproduction, crossover, and mutation operators.

The GA is used to minimize the cost function in Eq. (14), where cost function is the inverse of channel capacity for WLAN system. Through repeated applications of reproduction, crossover, and mutation operators, the initial population is transformed into a new population in an iterative manner. New populations will contain increasingly better chromosomes and will eventually converge to an optimal population that consists of the optimal chromosomes.

As for the GA calculations, each chromosome is assigned information of the position of transmitter as the optimization variables. A binary GA is applied and a population of 30 chromosomes is used at each generation. For each generated chromosome, the GA reruns the ray tracing program to calculate the channel capacity for each receiver from the given location of transmitter provided by the chromosome. In our simulation, when the channel capacity is bigger than the threshold value or GA do not find a better individual within 300 successive generations. The GA will be terminated and a solution is then obtained.

3 Numerical Results

Simulation scenarios and numerical results are presented in this section. A ray-tracing technique is developed to calculate the channel frequency response from 59.5 to 60.5 GHz with frequency interval of 5 MHz. i.e., 201 frequency components are used. The channel capacities for different transceiver positions in the indoor environments are investigated. Figure 4 is the top view ofthe indoor environment with dimensions of 10 m (Length) × 9.2 m (Width) × 3 m (Height). The floors and ceilings with 0.5 m thickness are both concrete material. The transmitting and receiving antenna are modeled as a antenna with simple omnidirectional radiation pattern and vertically polarized. Each antenna is with a fixed height of 1 m. The heights of desk, partition and file cabinet are 0.73, 3 and 1.7 m respectively. The thickness of partition is 0.115 m. Since the same materials for different frequencies
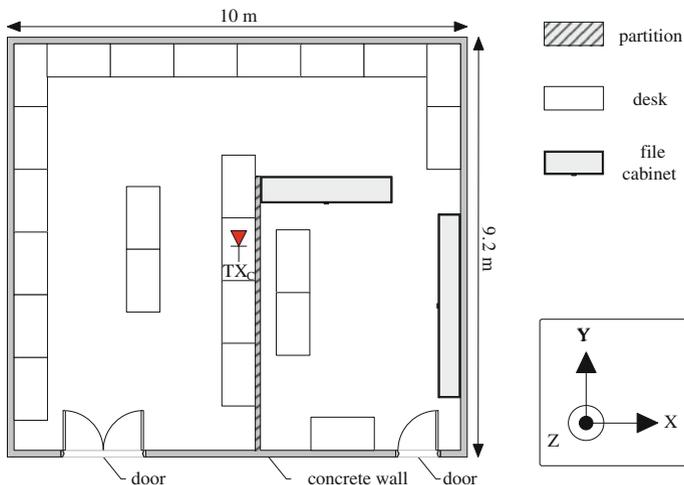

Fig. 4 Layout of a small personal communication environment

will have different propagation characteristics. Therefore, the frequency dependence of the dielectric and conductivity of materials is carefully considered in the channel simulation. The frequency response of the indoor environment was calculated by SBR/Image method for the 3×3 MIMO-WLAN channel. The number of ray tubes shooting from transmitter is 18,000. The maximum number of bounces setting beforehand is five, and the convergence is confirmed. The optimal antenna location for maximizing the channel capacity is searched by DDE and GA. The relative coefficient of the DDE are set as below: The scaling factors of F and λ both are 0.8 and the crossover rate $CR = 0.6$. The population size $N_p = 30$. The relative coefficient of the GA are set as below: The crossover rate $G_r = 0.6$. The mutation probability $G_M = 0.025$ and the population size $G_P = 30$. Two cases with different transceiver positions are considered in our simulation. The transmitting antenna TX$_C$ (5.25, 5, 1 m) located in the center of the indoor environment with a fixed height of 1m is used for our reference, as shown in Fig. 4.

A three-dimensional SBR/Image technique combined algorithm has been presented in this paper. This technique is used to calculate the WLAN channel impulse response for each location of the receiver. Based on the channel impulse response, the number of multipath components, the root mean square (RMS) delay spread τ_{RMS} and the mean excess delay τ_{MED} are computed.

The root mean square (RMS) delay spread τ_{rms} is defined as [33]:

$$\tau_{rms} = \sqrt{\frac{\sum_{n=1}^{N} \tau_n^2 |a_n|^2}{G} - \left(\frac{\sum_{n=1}^{N} \tau_n |a_n|^2}{G}\right)^2} \tag{15}$$

where $G = \sum_{n=1}^{N} |a_n|^2$ is the total multi-path gain.

The mean excess delay, $\overline{\tau}$ is defined as [33]:

$$\overline{\tau} = \frac{\sum_{n=1}^{N} \tau_n |a_n|^2}{G} \tag{16}$$

By Eqs. (15) and (16), we can obtain the RMS delay spreads and mean excess delay.

We compare the effects of TX$_C$, TX$_{DDE}$ and TX$_{GA}$ on 3×3 MIMO-WLAN transmission. For the first case, the transmitter is mobile in the whole indoor environment and the receivers are located on the tables with uniform intervals distribution, which 120 measurements with 0.5m spacing between adjacent points are carried out (e.g. transmission from a cell phone to a computer). The optimal locations of the transmitting antennas are at TX$_{DDE}$ (3.7, 3.42, 1 m) and TX$_{GA}$ (2.82, 4.73, 1 m) by using the DDE and GA, respectively. The channel capacity versus SNR is calculated, as shown in Fig. 5. Here SNR is defined as the ratio of the average transmitted power to the noise power at the front end of the receiver. It is seen that the channel capacity at SNR $= 40$ dB are about 12.58, 14.14 and 13.17 for TX$_C$, TX$_{DDE}$ and TX$_{GA}$ respectively. It is clear that channel capacity increased by DDE is better than those by GA about 7.4 %. The performance for the antenna location by DDE is better than that by GA.

The cost functions versus generation DDE and GA are calculated, as shown in Fig. 6. It is seen that the final cost function is reduced and good convergences are achieved less than 100 generations. It also shows that the convergent speed for the DDE is faster than that for GA.

In order to determine the multipath effect, the τ_{RMS} and τ_{MED} were calculated. A summary of these values are given in Table 1 for Scenarios I. For the receivers located on the tables case in Scenario I, the τ_{RMS} for TX$_C$, Tx$_{DDE}$ and TX$_{GA}$ are 4.63, 3.32 and 3.29 ns respectively. It is clear that the τ_{RMS} for the TX$_C$ case is the biggest.

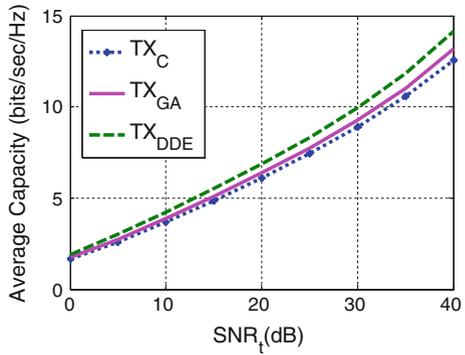**Fig. 5** Capacity versus SNR for the Scenario I

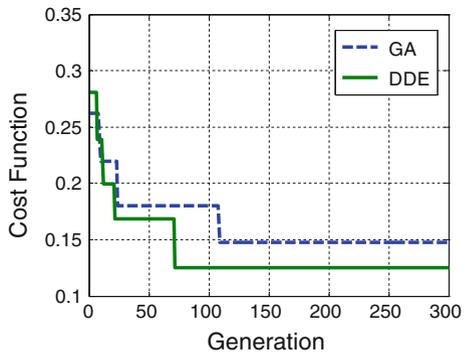**Fig. 6** Channel capacity average versus generation for the by DDE

Table 1 Mean excess delays and RMS delay spreads for the Scenarios I and II

Scenarios	Transmitting antennas					
	TX_C		TX_{GA}		TX_{DDE}	
	τ_{MED} (ns)	τ_{RMS} (ns)	τ_{MED} (ns)	τ_{RMS} (ns)	τ_{MED} (ns)	τ_{RMS} (ns)
Scenario I (Receivers located on the tables)	1.10	4.63	0.99	3.29	0.94	3.32
Scenario II (Receivers located in the whole indoor environment)	2.35	5.62	2.16	5.56	1.73	5.32

For the second case, the transmitter is mobile and the receivers are with uniform intervals distribution in the whole indoor environment, which 120 measurements with 0.9 m spacing between adjacent points were carried out (e.g. transmission from one cell phone to the other cell phone). The optimal locations of the transmitting antennas are at TX_{DDE} (2.64, 4.15, 1 m) and TX_{GA} (2.05, 2.35, 1 m) by using the DDE and GA, respectively.

The channel capacity versus SNR is calculated, as shown in Fig. 7. It is seen that the channel capacity at SNR = 40 dB are about 8.97, 13.82 and 12.46 for TX_c, TX_{DDE} and TX_{GA} respectively. It is clear that channel capacity increase by DDE is better than those by GA about 10.9 %. The performance for the antenna location by DDE is much better than that by GA.

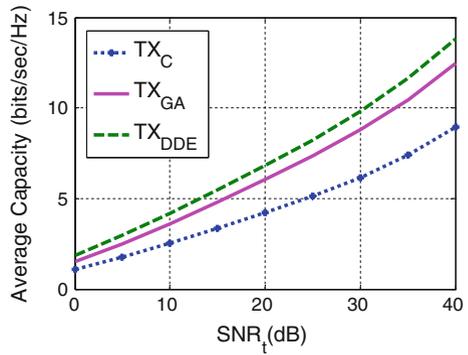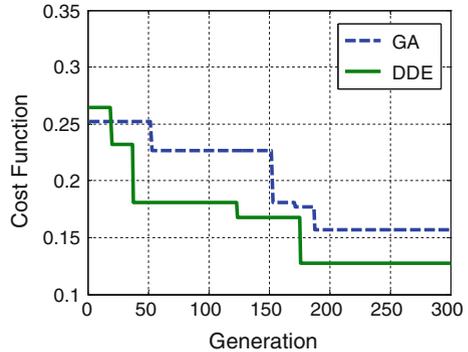**Fig. 7** Capacity versus SNR for the Scenario II

Fig. 8 Channel capacity average versus generation for the Scenario II by DDE

The cost functions for DDE and GA versus generation are calculated, as shown in Fig. 8. It is seen that the final cost function is reduced by DDE and good convergences are achieved less than 200 generations. It also shows that the convergent speed for the DDE is faster than that for GA.

For the receivers located in the whole indoor environment in Scenario II, the τ_{RMS} for TX_C, TX_{DDE} and TX_{GA} is 5.62, 5.32 and 5.56 ns respectively. It is clear that τ_{RMS} for the TX_C case is the biggest. A summary of these values are given in Table 1 for the Scenario II, which clearly shows the increase for the TX_C case.

4 Conclusions

The study has shown that we can deploy antenna location by DDE and GA to improve wireless communication system performance in real environment. By using the frequency responses of these MIMO channels, the channel capacity performance for Shannon–Hartley theorem WLAN communication system is calculated. Channel capacity is the average performance criteria for digital transmission system. The DDE and GA is used to maximizing the channel capacity. The frequency dependence of materials utilized in the structure in the indoor channel is accounted for in the channel simulation. i.e., the dielectric constant and loss tangent of obstacles are not assumed to be frequency independent. Numerical results show that channel capacity in two cases can be increased. It is also found that the channel capacity increased by DDE is better than that by GA.

References

1. Sato, K., Ihara, T., Saito, H., Tanaka, T., Sugai, K., Ohmi, N., et al. (1997). Measurements of reflection and transmission characteristics of interior structures of office buildings in the 60 GHz band. *IEEE Transactions on Antennas and Propagation*, *45*(12), 1783–1792.
2. Smulders, P. (2002). Exploiting the 60 GHz band for local wireless multimedia access: prospects and future directions. *IEEE Communications Magazine*, *40*(1), 140–147.
3. IEEE Standard for Information Technology—Telecommunications and information exchange between systems—Local and metropolitan area networks—Specific requirements—Part 11: Wireless LAN Medium Access Control (MAC) and Physical Layer (PHY) Specifications—2007. IEEE Standard 802.11-2007.
4. Wong, A. H., Neve, M. J., & Sowerby, K. W. (2007). Antenna selection and deployment strategies for indoor wireless communication systems. *IET Communications*, *1*(4), 732–738.
5. Lee, D. C. K., Neve, M. J., & Sowerby, K. W. (2007). The impact of structural shielding on the performance of wireless systems in a single-floor office building. *IEEE Transactions on Wireless Communications*, *6*(5), 1787–1795.
6. Yun, Z., Kim, S., & Iskander, M. (2008). An integrated method of ray tracing and genetic algorithm for optimizing coverage in indoor wireless networks. *IEEE Transactions on Antennas Wireless Propagation Letters*, *7*, 145–148.
7. Grubisic, S., Carpes, W. P., Jr, & Bastos, J. P. A. (2009). Optimization model for antenna positioning in indoor environments using 2-D ray-tracing technique associated to a real-coded genetic algorithm. *IEEE Transactions on Magnetics*, *45*(3), 1626–1629.
8. Chen, S. H., & Jeng, S. K. (1995). An SBR/image approach for indoor radio propagation in a corridor. *IEICE Transactions on Electronics*, *E78*, 1058–1062.
9. Chen, S. H., & Jeng, S. K. (1996). SBR image approach for radio wave propagation in tunnels with and without traffic. *IEEE Transactions Vehicular Technology*, *45*, 570–578.
10. Zhao, Y., Hao, Y., Alomainy, A., & Parini, C. (2006). UWB on-body radio channel modeling using ray theory and subband FDTD method. *IEEE Transactions Microwave Theory and Techniques, 153*(1), 120–126 (2006).
11. Zhang, Y., & Brown, A. K. (2006). Complex multipath effects in UWB communication channels. *IEE Proceedings Communications*, *153*(1), 120–126.
12. Richardson, P. C., Xiang, W., & Stark, W. (2006). Modeling of ultra-wideband channels within vehicles. *IEEE Journal on Selected Areas in Communications*, *24*(4), 906–912.
13. Driessen, P. F., & Foschini, G. J. (1999). On the capacity formula for multiple input-multiple output wireless channels: A geometric interpretation. *IEEE Transations on Communications*, *47*(2), 173–176.
14. Tila, F., Shepherd, P. R., & Pennock, S. R. (2004). Theoretical capacity evaluation of indoor micro- and macro-MIMO systems at 5 GHz using site specific ray tracing. *6th Electronics Letters*, *39*(5), 471–472.
15. Oh, S. H., & Myung, N. H. (2004). MIMO channel estimation method using ray-tracing propagation model. *14th Electronics Letters, 40*(21), 1350–1352.
16. Loredo, S., & Rodríguez-Alonso, A. (2008). Indoor MIMO channel modeling by rigorous GO/UTD-based ray tracing. *IEEE Transactions on Vehicular Technology*, *57*(2), 680–692.
17. Chen, S. H., & Jeng, S. K. (1997). An SBR/image approach for radio wave propagation in indoor environments with metallic furniture. *IEEE Transactions on Antennas Propagation*, *45*(1), 98–106.
18. Balanis, C. A. (1989). *Advanced engineering electromagnetics*. Hoboken: Wiley.
19. Iskander, M. F., & Yun, Z. (2002). Propagation prediction models for wireless communication systems. *IEEE Transactions on Microwave Theory and Technique, 50*(3).
20. Oppermann, I., Hamalainen, M., & Iinatti, J. (2004). *UWB theory and applications*. Hoboken: Wiley.
21. Kamen, E. W., & Heck, B. S. (2000). *Fundamentals of signals and systems using the web and matlab*. New Jersey: Prentice-Hall.
22. Gabriella, M., Benedetto, D., & Giancola, G. (2004). *Understanding ultra wide band radio fundamentals*. New Jersey: Prentice Hall.
23. Loredo, S., & Rodríguez-Alonso, A. (2008). Indoor MIMO channel modeling by rigorous GO/UTD-based ray tracing. *IEEE Transactions on Vehicular Technology*, *57*(2), 680–692.
24. Malik, W. Q., Stevens, C. J., & Edwards, D. J. (2007). Spatio-temporal ultrawideband indoor propagation modeling by reduced complexity geometric optics. *IEET Communications*, *1*(4), 751–759.
25. Strang, G. (1988). *Linear algebra and its applications*. San Diego: Harcourt Brace Jovanovich.
26. Balanis, C. A. (1989). *Advanced engineering electromagnetics*. USA: Wiley.
27. Xu, Z., Sfar, S., & Blum, R. S. (2009). Analysis of MIMO systems with receive antenna selection in spatially correlated Rayleigh fading channels. *IEEE Transations on Vehicular Technology*, *58*(1), 251–262.

28. Chang, W.-J., T, Jenn-Hwan, & Peng, S.-Y. (2008). Frequency-space-polarization on UWB MIMO performance for body area network applications. *IEEE Antennas and Wireless Propagation Letters*, 7, 577–580.

29. Valenzuela-Valdés, J. F., García-Fernández, M. A., Martínez-González, A. M., & Sánchez-Hernández, D. A. (2008). The influence of efficiency on receive diversity and MIMO capacity for Rayleigh-fading channels. *IEEE Transactions Antennas and Propagattion*, 56(5), 1444–1450.

30. Storn, R., & Price, K. (1995). Differential evolution—a simple and efficient adaptive scheme for global optimization over continuous spaces. Technical Report TR-95-012, International Computer Science Institute, Berkeley.

31. Goldberg, D. E. (1989). *Genetic algorithm in search optimization and machine learning*. Boston: Addison Wesley.

32. Johnson, J. M., & Rahmat-Samii, Y. (1997). Genetic algorithms in engineering electromagnetics. *IEEE Antennas and Propagation Magazine*, 39(4), 7–21.

33. Rappaport, T. S. (2002). *Wireless communications: Principles and practice 2nd ed*. Upper Saddle River, NJ, USA: Prentice Hall PTR.

Author Biographies

Shu-Han Liao was born in Taipei, Taiwan, Republic of China, on September 18, 1982. He received the M.S.C.E. degree from Feng Chia University in 2008, and now is working toward Ph.D. degrees in the Department of Electrical Engineering, Tamkang University. His current research interests include indoor wireless communication systems, ultra-wideband systems, and MIMO systems.

Chien-Ching Chiu received his BSCE degree from National Chiao Tung University, Hsinchu, Taiwan, in 1985 and his MSEE and Ph.D. degrees from National Taiwan University, Taipei, in 1987 and 1991, respectively. From 1987 to 1989, he was a communication officer with the ROC Army Force. In 1992 he joined the faculty of the Department of Electrical Engineering, Tamkang University, where he is now a professor. From 1998 to 1999, he was a visiting scholar at the Massachusetts Institute of Technology, Cambridge, and the University of Illinois at Urbana-Champaign. He is a visiting professor with the University of Wollongong, Australia, in 2006. Moreover, he was a visiting professor with the University of London, United Kingdom, in 2011.His current research interests include microwave imaging, numerical techniques in electromagnetics, indoor wireless communications, and ultra-wideband communication systems. He has published more than 90 journal papers on inverse scattering problems, communication systems and optimization algorithms.

Min-Hui Ho was born in Taipei, Taiwan, Republic of China, on March 30, 1983. She is working toward Ph.D. degree in the Department of Electrical Engineering, Tamkang University, Tamsui, Taipei, Taiwan, R.O.C. Her current research interests include indoor wireless communication systems and ultra-wideband systems.